Diffractive charmonium spectrum in high energy collisions in the basis light-front quantization approach

Guangyao Chen, Yang Li*, Pieter Maris, Kirill Tuchin, James P. Vary

Department of Physics and Astronomy, Iowa State University, Ames, IA 50011, USA

arXiv:1610.04945v1 [nucl-th] 17 Oct 2016

Abstract

Using the charmonium light-front wavefunctions obtained by diagonalizing an effective Hamiltonian with the one-gluon exchange interaction and a confining potential inspired by light-front holography in the basis light-front quantization formalism, we compute production of charmonium states in diffractive deep inelastic scattering and ultra-peripheral heavy ion collisions within the dipole picture. Our method allows us to predict yields of all excited charmonium and bottomonium states below the open flavor thresholds in high-energy deep inelastic scattering, proton-nucleus and ultra-peripheral heavy ion collisions. The obtained charmonium cross section is in reasonable agreement with experimental data at HERA, RHIC and LHC. We observe that the cross-section ratio $\sigma_{\Psi(2s)}/\sigma_{J/\Psi}$ reveals significant independence of model parameters.

Keywords: heavy quarkonium, light front, holographic QCD, dipole model

1. Introduction

Exclusive vector meson production in deep inelastic scattering (DIS) and deeply virtual Compton scattering (DVCS) are effective tools for studying Quantum Chromodynamics (QCD) [1]. At low x these processes are dominated by gluon saturation [2, 3]. Models incorporating the saturation physics successfully describe the high precision data harvested at Hadron-Electron Ring Accelerator (HERA) [4–9] and are instrumental for deriving predictions for future experiments at LHeC [10] and EIC [11]. Theoretical calculations often employ the dipole model [12, 13] that relies on the separation of scales: in the proton rest frame, the lifetime of the virtual photon is much longer than the time scale of the interaction, and much shorter than the quarkonium formation time. It was used in Refs. [14, 15] to describe both exclusive and diffractive HERA measurements at low x.

The largest theoretical uncertainty in the calculation of diffractive heavy quarkonium production in the dipole picture arises from poor knowledge of the heavy quarkonium light-front wavefunction (LFWF). In phenomenological applications, the LFWFs are simply educated guesses with several free parameters [7, 14]. While such phenomenological models can be successful in explaining the experimental data, the abundance of free parameters limits the predictive power. With the electron-ion collider on the horizon, where around 30% of total events are expected to be diffractive, finding well-constrained heavy quarkonium LFWFs based on the dynamics of QCD becomes important.

Fortunately, recent progress in the basis light-front quantization (BLFQ) approach [16–18] has paved an avenue for improving the understanding of the heavy quarkonium system. It has enabled the computation of the LFWFs for any heavy quarkonium state and thus calculate the corresponding diffractive cross sections. The BLFQ approach has been successfully applied to calculate the electron anomalous magnetic moment [17, 19], and to study the positronium system [20, 21]. Recently, some of us employed the light-front Hamiltonian formalism to obtain the mass spectrum for charmonium and bottomonium. This was

*Corresponding author

Email addresses: gchen@iastate.edu (Guangyao Chen), leeyoung@iastate.edu (Yang Li), pmaris@iastate.edu (Pieter Maris), tuchin@iastate.edu (Kirill Tuchin), jvary@iastate.edu (James P. Vary)

achieved by diagonalizing an effective Hamiltonian that incorporates the one-gluon exchange interaction and a confining potential inspired by light-front holography [22]. The decay constants and the charge form factors for selected eigenstates calculated using the corresponding LFWFs are comparable to the experimental measurements as well as to results from Lattice QCD and Dyson-Schwinger Equation approaches. Compared to phenomenological LFWFs used in the literature, LFWFs from the BLFQ approach possess appealing merits. In particular, the LFWFs arise from successful fits to the heavy quarkonia mass spectroscopy, show success in applications to decay constants and provide predictions for additional quantities such as charge form factors all within the same formalism.

The main goal of this letter is to compute the diffractive cross sections for the heavy quarkonium production at low x using the dipole model to take into account the gluon saturation and employing the theoretically sound and phenomenologically constrained light-front wavefunctions computed in the BLFQ formalism.

2. Background

In the dipole model, the amplitude for exclusive heavy quarkonium production in DIS can be calculated as [14]

$$\mathcal{A}_{T,L}^{\gamma^* p\to Ep}(x,Q,\Delta) = \mathrm{i}\int \mathrm{d}^2\boldsymbol{r}\int_0^1 \frac{\mathrm{d}z}{4\pi}\int \mathrm{d}^2\boldsymbol{b}\,(\Psi_E^*\Psi)_{T,L}(r,z,Q)\,\mathrm{e}^{-\mathrm{i}[\boldsymbol{b}-(1-z)\boldsymbol{r}]\cdot\boldsymbol{\Delta}}\,\frac{\mathrm{d}\sigma_{q\bar{q}}}{\mathrm{d}^2\boldsymbol{b}}(x,r)\,, \tag{1}$$

where T and L denote the transverse and longitudinal polarization of the virtual photon (with virtuality Q^2) and the produced quarkonium, and $t=-\boldsymbol{\Delta}^2$ denotes the momentum transfer. On the right-hand side, $\boldsymbol{r}$ is the transverse size of the color dipole, z is the LF longitudinal momentum fraction of the quark, $\boldsymbol{b}$ is the impact parameter of the dipole relative to the proton and x is the Bjorken variable. Ψ and Ψ_E^* are LFWFs of the virtual photon and the exclusively produced quarkonium respectively. The cross section is relative to the amplitude as

$$\frac{\mathrm{d}\sigma_{T,L}^{\gamma^* p\to Ep}}{\mathrm{d}t} = \frac{1}{16\pi}|\mathcal{A}_{T,L}^{\gamma^* p\to Ep}(x,Q,\Delta)|^2\,. \tag{2}$$

Furthermore, several phenomenological corrections are needed in order to describe the experimental data. For example, the contribution from the imaginary part of the scattering amplitude is conventionally corrected by multiplying the cross section by a factor $(1+\beta^2)$ [14], where β is the ratio of the imaginary and real parts of the scattering amplitude, and is calculated as [23]

$$\beta = \tan(\pi\lambda/2), \quad \text{with} \quad \lambda \equiv \frac{\partial \ln\left(\mathcal{A}_{T,L}^{\gamma^* p\to Ep}\right)}{\partial \ln(1/x)}. \tag{3}$$

The skewedness correction, which takes into account the fact that two gluons interacting with the dipole are carrying slightly different momentum fractions, will be specified in Sec. 2.1, since it have been implemented differently for different dipole models in the literature.

2.1. Dipole cross section parametrizations

There are many dipole cross section parametrizations available in the literature based on different theoretical considerations and inspired by the GBW model [4]. For this study we employ two representative dipole parametrizations: the impact parameter dependent saturation model (bSat) [7] and the impact parameter dependent Color Glass Condensate model (bCGC) [9] to take advantage of their explicit impact parameter dependence, which is important in diffractive quarkonium production.

The bSat dipole model is based on the Glauber-Mueller formula [12] and assumes the dipole cross section as follows,

$$\frac{\mathrm{d}\sigma_{q\bar{q}}}{\mathrm{d}^2\boldsymbol{b}} = 2\left[1-\exp\left(-\frac{\pi^2}{2N_c}r^2\alpha_s(\mu^2)xg(x,\mu^2)T(b)\right)\right], \tag{4}$$

Model	Q^2/GeV^2	N_f	$m_{u,d,s}/\mathrm{GeV}$	m_c/GeV	μ_0^2/GeV^2	A_g	λ_g	$\chi^2/\mathrm{d.o.f.}$
bSat I	[0.25,650]	3	0.14	1.4	1.17	2.55	0.020	$193.0/160 = 1.21$
bSat II	[0.25,650]	3	0.14	1.35	1.20	2.51	0.024	$190.2/160 = 1.19$
bSat III	[0.25,650]	3	0.14	1.5	1.11	2.64	0.011	$198.1/160 = 1.24$
bSat IV	[0.75,650]	4	≈ 0	1.27	1.51	2.308	0.058	$298.89/259 = 1.15$
bSat V	[0.75,650]	4	≈ 0	1.4	1.11	2.373	0.052	$316.61/259 = 1.22$

Table 1: Parameters of the initial gluon distribution in the bSat model in Eq. (5) determined from fits to F_2 data. Parameters of the bSat I-III are fitted to ZEUS data only [14]. Parameters of the bSat IV and V are fitted to combined HERA data [25] .

Model	$B_{\mathrm{CGC}}/\mathrm{GeV}^{-2}$	m_c/GeV	γ_s	$\mathcal{N}_0$	x_0	λ_s	$\chi^2/\mathrm{d.o.f.}$
bCGC I	5.591	1.4	0.7376	0.7	1.632×10^{-5}	0.2197	$144.0/160 = 0.900$
bCGC II	5.5	1.27	0.6599	0.3358	0.00105	0.2063	$368.4/297 = 1.241$
bCGC III	5.5	1.4	0.7376	0.3658	0.00069	0.2023	$370.9/297 = 1.249$

Table 2: Parameters of the bCGC model in Eq. (7) determined from fits to F_2 data. Parameters in the bCGC I are fitted to ZEUS data only [32]. Parameters of the bCGC II and III are fitted to combined HERA data [33] .

where $T(b)$ is the proton shape function, which is assumed to be Gaussian, $T_G(b) = \exp(-b^2/2B_G)/(2\pi B_G)$, with $B_G = 4\ \mathrm{GeV}^{-2}$. α_s is determined using LO evolution of the running coupling constant, with fixed number of flavors N_f. μ^2 is related to the dipole size r through $\mu^2 = 4/r^2 + \mu_0^2$. The gluon density is determined using LO DGLAP evolution [24] from an initial scale μ_0^2, where the initial gluon density is,

$$xg(x,\mu_0^2) = A_g\, x^{-\lambda_g}\,(1-x)^{5.6}. \tag{5}$$

In the bSat dipole model, μ_0, A_g and λ_g are parameters to be determined by the inclusive DIS data. We use parametrizations given in Ref. [14, 25] for this investigation, which we provide in Table 1. We follow the prescription in Ref. [14] for the skewedness correction in the bSat dipole model. R_{bSat} is assumed to be

$$R_{\mathrm{bSat}}(\delta_{bSat}) = \frac{2^{2\delta_{\mathrm{bSat}}+3}}{\sqrt{\pi}}\frac{\Gamma(\delta_{\mathrm{bSat}}+5/2)}{\Gamma(\delta_{\mathrm{bSat}}+4)} \quad \text{with} \quad \delta_{\mathrm{bSat}} \equiv \frac{\partial \ln\left[xg(x,\mu^2)\right]}{\partial \ln(1/x)}. \tag{6}$$

The obtained R_{bSat} is then applied multiplicatively to the gluon density function in Eq. (4). Such prescription of skewedness correction is also adopted in Ref. [25–28].

The bCGC dipole model is a smooth interpolation of the solutions of the BFKL equation [29] for small dipole sizes and the Levin-Tuchin solution [30] of the BK equation [31] deep inside the saturation region for larger dipoles,

$$\frac{\mathrm{d}\sigma_{q\bar{q}}}{\mathrm{d}^2\boldsymbol{b}} = 2\mathcal{N}(rQ_s,x) = 2\begin{cases} \mathcal{N}_0\left(\frac{rQ_s}{2}\right)^{2\left(\gamma_s+\frac{1}{\kappa_s\lambda_s}\frac{\ln\frac{2}{rQ_s}}{\ln(1/x)}\right)} & : \quad rQ_s \le 2 \\ 1-\mathrm{e}^{-\mathcal{A}\ln^2(\mathcal{B}rQ_s)} & : \quad rQ_s > 2 \end{cases}, \tag{7}$$

with $Q_s \equiv Q_s(x) = (x_0/x)^{\lambda_s/2}Q_0$, where $Q_0 = 1$ GeV. γ_s, κ_s, λ_s are parameters to be determined by inclusive DIS data. $\mathcal{A}$ and $\mathcal{B}$ should be evaluated by continuity conditions at $rQ_s = 2$. We use the parametrization by Soyez [32] and two parametrizations in Ref. [33] for this investigation, which we provide in Table 2. Note that different conventions were used for the impact parameter dependence in Ref. [32, 33]. We follow the prescription in Ref. [33, 34] for the skewedness correction in the bCGC dipole model. R_{bCGC} is assumed to be,

$$R_{\mathrm{bCGC}}(\delta_{\mathrm{bCGC}}) = \frac{2^{2\delta_{\mathrm{bCGC}}+3}}{\sqrt{\pi}}\frac{\Gamma(\delta_{\mathrm{bCGC}}+5/2)}{\Gamma(\delta_{\mathrm{bCGC}}+4)} \quad \text{with} \quad \delta_{\mathrm{bCGC}} \equiv \frac{\partial \ln\left(\mathcal{A}_{T,L}^{\gamma^* p\to Ep}\right)}{\partial \ln(1/x)}. \tag{8}$$

The obtained R_{bCGC} is then applied multiplicatively to the production amplitude.

2.2. Heavy quarkonium in a holographic basis

Most phenomenological vector meson LFWFs used in the literature are based on analogy with the virtual photon LFWF, which can be evaluated perturbatively [35]. It is generally assumed that the vector meson is predominantly in the leading quark-antiquark Fock state and its spin and polarization structures are the same as in the virtual photon case [36]. Phenomenological wavefunctions differ by the specification of the scalar components of the LFWFs. For example, the boosted Gaussian (bG) [37, 38] LFWFs are obtained by boosting the momentum distribution of the quark inside the meson to the infinite momentum frame from the meson rest frame, assuming the momentum distribution of the quark is Gaussian in the meson rest frame.

The basis light-front quantization formalism offers a rigorous approach for the vector meson LFWFs. In principle, the eigenvalue equation of the light-front quantized QCD Hamiltonian directly produces the hadron mass spectrum of and the LFWFs

$$H_{\rm LFQCD}|\psi_h\rangle = M_h^2|\psi_h\rangle, \quad (H_{\rm LFQCD} \equiv P^+\hat{P}^-_{\rm LFQCD} - \vec{P}^2)\ . \tag{9}$$

However, it is a formidable task to work with the full QCD Hamiltonian based on our current knowledge of QCD in the non-perturbative regime. On the other hand, it has been shown [22] that the following effective Hamiltonian, combining the holographic QCD Hamiltonian and the one-gluon exchange dynamics, produces the heavy quarkonia spectroscopy,

$$H_{\rm eff} = \frac{\boldsymbol{k}_\perp^2 + m_q^2}{z(1-z)} + \kappa_{\rm con}^4\boldsymbol{\zeta}_\perp^2 - \frac{\kappa_{\rm con}^4}{4m_q^2}\partial_z\big(z(1-z)\partial_z\big) - \frac{4\pi C_F\alpha_s}{Q^2}\bar{u}_s(k)\gamma_\mu u_{s'}(k')\bar{v}_{\bar{s}'}(\bar{k}')\gamma^\mu v_{\bar{s}}(\bar{k})\ , \tag{10}$$

where $C_F = \frac{4}{3}$, $Q^2 = -\frac{1}{2}(k'-k)^2 - \frac{1}{2}(\bar{k}-\bar{k}')^2$. The last term is the one-gluon exchange interaction derived from the QCD Lagrangian, and provides the short-distance physics and spin structures needed for the hyperfine splitting. The rest of the Hamiltonian is developed based on soft-wall light-front holographic QCD [39], which dominates the long-distance physics and delivers an effective confinement in both transverse and longitudinal directions. The longitudinal confining potential in Eq. (10) was first proposed for heavy quarkonia by some of us in Ref. [22], implementing the pQCD asymptotics for the distribution amplitude (DA) at the endpoints, $\phi^{\rm DA}(x) \sim x^\alpha(1-x)^\beta$. The soft-wall AdS/QCD is implemented as a first approximation of QCD [39]. In Ref. [22], the model is solved in the basis function approach, and the (generalized) soft-wall wavefunctions $\phi_{nm}(\boldsymbol{k}_\perp/\sqrt{z(1-z)})$ and $\chi_l(z)$ are adopted as the basis functions:

$$\langle \boldsymbol{k}_\perp, z, s, \bar{s}|\psi_h\rangle \equiv \psi_{s\bar{s}}(\boldsymbol{k}_\perp, z) = \sum_{n,m,l} f_{nmls\bar{s}}\ \phi_{nm}(\boldsymbol{k}_\perp/\sqrt{z(1-z)})\chi_l(z), \tag{11}$$

where ϕ_{nm} and χ_l are analytically known functions[1] and the coefficients $f_{nmls\bar{s}}$ are obtained through diagonalization.

The model has three parameters. The strong coupling constant α_s is fixed, $\alpha_s(M_{c\bar{c}}) \simeq 0.36$ and $\alpha_s(M_{b\bar{b}}) \simeq 0.25$, related via pQCD evolution of the coupling constant. The effective quark mass m_q and the confining strength $\kappa_{\rm con}$ are determined by fitting the mass spectrum of the Hamiltonian to the experimental measurements. The calculated charmonium ($m_c = 1.522$ GeV and $\kappa_{\rm con} = 0.938$ GeV) and bottomonium ($m_b = 4.763$ GeV and $\kappa_{\rm con} = 1.490$ GeV) spectra agree with the experimental values within a root-mean-square deviation of 50 MeV for the states below the open flavor thresholds. The resulting light-front wavefunctions are used to calculate the decay constants, the form factors and the charge radii. The results compare reasonably well with the experiments and other established methods (Lattice QCD and Dyson-Schwinger Equations). Overall, this model improves the soft-wall light-front holographic QCD results.

We interpret the quark mass obtained by the fitting as the effective quark mass in the meson bound state, which is not necessarily the same as the current quark mass in the virtual photon LFWF and the dipole cross section. In this investigation, we choose the quark mass in the virtual photon LFWF

[1] In particular, the soft-wall wavefunction ϕ_{nm} is the harmonic oscillator function in holographic variable $\boldsymbol{k}_\perp/\sqrt{z(1-z)}$, which is a generalization of the boosted Gaussian wavefunction.

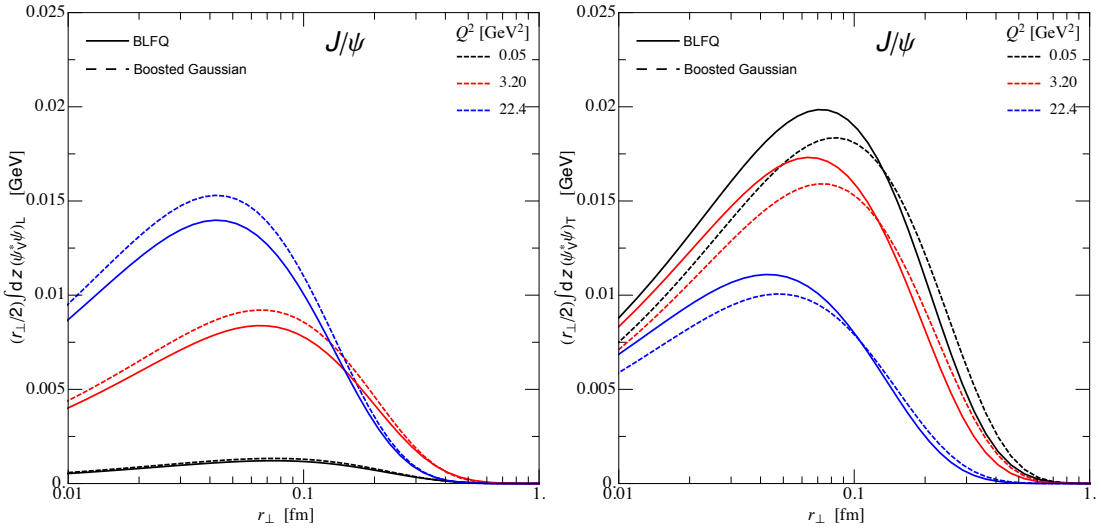

Figure 1: (Colors online) The longitudinal (*Left*) and transverse (*Right*) overlap functions between the J/Ψ LFWF and the photon LFWF predicted by the BLFQ LFWF and boosted Gaussian LFWF for three representative values of Q^2. The BLFQ LFWF is obtained by diagonalizing the effective Hamiltonian in Eq. (10) [22]. The boosted Gaussian LFWF is given in Ref. [14]. The charm quark mass in the photon LFWF is set to be $m_c = 1.4$ GeV.

according to the dipole cross section parametrization. In Fig. 1, we present the overlap function between the J/Ψ LFWF and the photon LFWF integrated over z as predicted by the BLFQ LFWF and the boosted Gaussian LFWF as a function of transverse separation of the quark and antiquark. The BLFQ LFWF is obtained by diagonalizing the effective Hamiltonian in Eq. (10), as mentioned [22]. The boosted Gaussian LFWF is given in Ref. [14]. The charm quark mass in the photon LFWF is set to be $m_c = 1.4$ GeV. In this investigation, we focus on comparing the prediction of the BLFQ LFWF to experiments. We use the prediction of boosted Gaussian model [14, 40] as reference.

Comparing to LFWFs from phenomenological models, e.g., the boosted Gaussian model, the heavy quarkonium LFWF from the BLFQ approach is constrained by a variety of observables. It also provides direct access to higher excited states without introducing additional assumptions, e.g., the normalization and orthogonality conditions are fulfilled automatically. Moreover, within the BLFQ framework, it is straightforward to extend the LFWF to include higher Fock sectors, e.g., the quark-antiquark-gluon sector.

3. Charmonium production at HERA

We calculate charmonium production using five sets of parameters in the bSat dipole model [14, 25] and three sets of parameters in the bCGC dipole model [32, 33] using the BLFQ charmonium LFWF in the kinematic range of the HERA experiment [41–43]. Various cross sections obtained as a function of the kinematic variables Q^2, W and t are in reasonable agreement with experimental data. As an illustration, we present some representative results using the BLFQ and the boosted Gaussian LFWFs in Fig. 2. The bSat I parametrization in Table 1 is implemented for the dipole cross section.

In the left panel of Fig. 2, solid and dashed curves give the total J/Ψ cross section as a function of $(Q^2 + M_V^2)$ predicted by the BLFQ and the boosted Gaussian LFWFs respectively. The photon-proton c.m. energy is $W = 90$ GeV. In the center panel of Fig. 2, solid and dashed curves give the total J/Ψ cross section as a function of various values of Q^2 and W predicted by the BLFQ and the boosted Gaussian LFWFs respectively. The boosted Gaussian LFWF parametrization in Ref. [14] gives excellent fits to the J/Ψ cross section measurements at HERA, if the bSat I parametrization is used for the dipole cross section. For the same dipole cross section parametrization, the BLFQ LFWF calculation underestimates the J/Ψ production at HERA. Nevertheless, except when Q^2 is very small, the predictions of the BLFQ

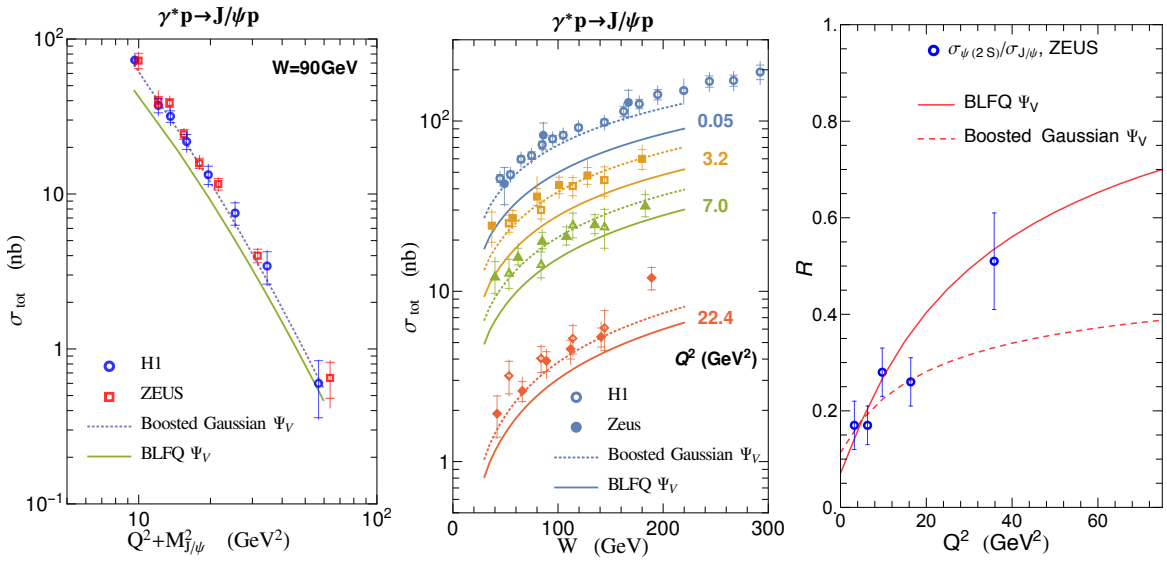

Figure 2: (Colors online) Using the b-Sat I parametrization in Table 1, predictions of the BLFQ LFWF (solid curves) and the boosted Gaussian LFWF (dashed curves) compare to the HERA experimental data. The calculations use boosted Gaussian LFWF can be found in Ref. [14]. *Left*: Total J/Ψ cross section for different value of $(Q^2 + M_V^2)$ at $W = 90$ GeV [41, 42]. The inner bars indicate the statistical uncertainties; the outer bars are the statistical and systematic uncertainties added in quadrature. *Middle*: Total J/Ψ cross section for different values of Q^2 and W [41, 42]. The inner bars indicate the statistical uncertainties; the outer bars are the statistical and systematic uncertainties added in quadrature. *Right*: Cross-section ratio $\sigma_{\Psi(2s)}/\sigma_{J/\Psi}$ for different Q^2. Error bars indicate the statistical uncertainties only [43].

LFWF are slightly lower than the experimental measurements, if we take statistical and systematic uncertainties into account.

The discrepancy with the HERA measurements at small Q^2 should not pose a major hindrance for the application of the BLFQ LFWF on diffractive charmonium production. The theoretical uncertainty in the dipole model is large at small Q^2. For the dipole cross section we employed, the photon wavefunction is calculated based on tree-level perturbative QED, without taking confinement and QCD corrections into account. The pQED photon wavefunction is more reliable at large spacelike values of Q^2, since contributions from large size dipoles are suppressed except at end point of z. However, confinement effects are likely to play an important role at small Q^2 [36]. For such reasons, the J/Ψ cross section at small Q^2 is clearly model dependent. Such uncertainty could be reduced by a consistent treatment of heavy quarkonium wavefunction and photon wavefuntion by including confinement and QCD corrections in the photon wavefunction.

In the right panel of Fig. 2, we compare the predictions of the BLFQ and the boosted Gaussian LFWFs for the $\sigma_{\Psi(2s)}/\sigma_{J/\Psi}$ cross-section ratio as a function of Q^2 in electron-proton scattering measured at HERA [43]. Solid and dashed curves are again the predictions of the BLFQ and the boosted Gaussian LFWFs respectively. Both predictions are within experimental uncertainty for moderate Q^2. The growing differences between the BLFQ and the boosted Gaussian results at larger Q^2 suggest the importance of additional data in this region to further distinguish between the LFWFs.

An accurate dipole cross section requires quantitative understanding of saturation in the small-x regime, which is not available currently. Observables with weak dipole cross section dependence are favored if one wants to test the validity of heavy quarkonium LFWFs. We will discuss the dipole model dependence of the charmonium cross section and cross-section ratio in Sec. 5.

4. Charmonium production at RHIC and LHC

Diffractive charmonium production can be studied using the ultra-peripheral heavy-ion collisions (UPC), in which two heavy ions scatter at large impact parameters. In the rest frame of one of the ions, the exclusive heavy quarkonium production in UPC can be regarded as a result of the scattering of equivalent photons of the incident ion off the target ion [44]. At low x the color dipole scatters coherently from the entire nucleus. The saturation effect is amplified by the large number of nucleons interacting with the dipole along its path through the nucleus.

The coherent diffractive heavy quarkonium production can be obtained by averaging over all possible states of nucleon configurations Ω of the nucleus. In the photon-nucleus collision, the corresponding diffractive heavy quarkonium production amplitude can be calculated by replacing the photon-proton dipole cross section $\mathrm{d}\sigma_{q\bar{q}}/\mathrm{d}^2\boldsymbol{b}$ in Eq. (1) with the nucleon configuration averaged dipole cross section [7],

$$\left\langle \frac{\mathrm{d}\sigma_{q\bar{q}}}{\mathrm{d}^2\boldsymbol{b}} \right\rangle_{\Omega} = 2\left[1 - \left(1 - \frac{T_A(\boldsymbol{b})}{2}\sigma^p_{q\bar{q}}\right)^A\right] , \tag{12}$$

where $\sigma^p_{q\bar{q}}$ is the photon-proton dipole cross section, integrated over the impact parameter, and A is the atomic number of the nucleus. T_A is the thickness profile of the nucleus in the transverse dimension, with $\boldsymbol{b}$ the impact parameter of the dipole relative to the nucleus. We adopt a Woods-Saxon profile for the nucleon distribution.

Extensive experimental data have been collected for heavy quarkonium production both at RHIC and LHC. The dipole picture has provided a reasonable explanation for the experimental data using phenomenological charmonium LFWFs, e. g., Ref. [28, 45–47]. In this section, we check the predictions of the BLFQ LFWF against measurements in Ref. [48–52] using bSat I in Table 1 and bCGC I in Table 2 as dipole cross section parametrizations. We also present the prediction of the boosted Gaussian LFWF as reference.

The latest measurement at RHIC for coherent J/Ψ production at mid-rapidity with two gold nuclei colliding at $\sqrt{s_{\mathrm{NN}}} = 200$ GeV provides a J/Ψ cross section $\mathrm{d}\sigma/\mathrm{d}y = 45.6 \pm 13.3$ (stat) ± 5.9 (sys) μb [49]. A previous study using the boosted Gaussian LFWFs and bSat I dipole parametrization provides a prediction of 109 μb [28]. Using the BLFQ LFWF, the bSat I dipole parametrization yields a prediction of 59.9 μb, while the bCGC I dipole parametrization provides a prediction of 52.6 μb. Both results are therefore consistent with the latest data within experimental uncertainty. Note that the kinematic region of the RHIC experiment corresponds to a photon-nucleon c.m. energy of 34 GeV, with the Bjorken-x roughly 0.15, which implies that the dipole picture is marginally applicable for such process at mid-rapidity.

The predictions of the BLFQ LFWF are also consistent with experimental data for coherent production of J/Ψ at mid-rapidity in ultra-peripheral Pb-Pb collisions at $\sqrt{s_{NN}} = 2.76$ TeV [50, 51]. In the left panel of Fig. 3, solid curves show the prediction of the BLFQ J/Ψ LFWF using bSat I (red) and bCGC I (blue) dipole model parametrizations. We find both of these results are within the statistical uncertainty of the experimental data. In contrast, dashed curves are the predictions of the boosted Gaussian LFWF of J/Ψ using bSat I (red) and bCGC I (blue) dipole model parametrizations. We find both of these overshoot the data.

Overall, the BLFQ LFWF gives a good fit to coherent J/Ψ production in UPC both at RHIC and LHC. The boosted Gaussian LFWF overestimates J/Ψ production in UPC although it gives a good fit to the HERA data.

The right panel of Fig. 3 shows the experimental result for coherent $\Psi(2s)$ production in ultra-peripheral Pb-Pb collisions at $\sqrt{s_{NN}} = 2.76$ TeV measured by the ALICE collaboration [52]. Solid curves present the prediction of the BLFQ $\Psi(2s)$ LFWF, with bSat I (red) and bCGC I (blue) for the dipole model parametrizations, and dashed curves are the prediction of the boosted Gaussian LFWF, with bSat I (red) and bCGC I (blue) as dipole model parametrizations respectively. Neither the BLFQ nor the boosted Gaussian LFWF is able to explain the experimental result. All of the presented results underestimate the $\Psi(2s)$ productions in UPC events. The cross-section ratio $\sigma_{\Psi(2s)}/\sigma_{J/\Psi}$ predicted by the dipole model is in agreement with electron-proton collision at $Q^2 = 0$. On the other hand, the same cross-section ratio measured by the ALICE experiment is almost twice as large as in photon-proton

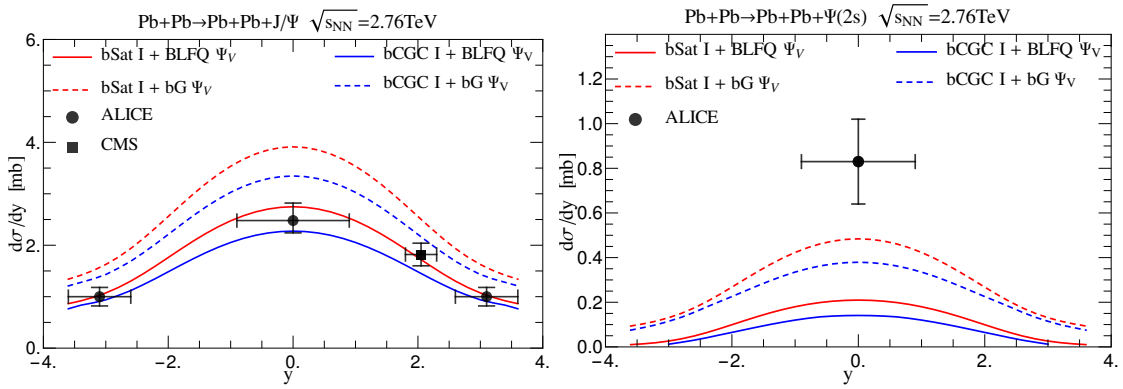

Figure 3: (Colors online) The predictions of the BLFQ LFWF (solid curves) and the boosted Gaussian LFWF (dashed curves) for the coherent production of J/Ψ (*Left*) and $\Psi(2s)$ (*Right*) production in ultra-peripheral collision at $\sqrt{s_{NN}} = 2.76$ TeV, compare to the measurements by the ALICE collaboration [50, 52] and CMS collaboration [51] at LHC. The bSat I parametrization (red curves) in Table 1 and the bCGC I parametrization (blue curves) in Table 2 are implemented as the dipole cross section. The calculations using the boosted Gaussian LFWFs can be found in Ref. [28]. Error bars show statistical uncertainties only.

collision experiments. Reductions in both theoretical and experimental uncertainties are needed for improving our knowledge of $\Psi(2s)$ production in UPC at LHC.

5. Dipole model dependence

In the dipole model, the cross section for the diffractive vector meson production is calculated through a convolution of the dipole cross section and the overlap of the vector meson LFWF and the photon LFWF. Consequently, it is expected that uncertainties from both the dipole cross section and the vector meson LFWF contribute to the uncertainty of the result. Inclusive data from the DIS experiment at HERA used to determine the dipole cross sections have large uncertainties in the small-x regime, which leads to large uncertainties in the dipole model parameters. State-of-the-art fits to the measured heavy quarkonium cross section measurement are not sufficient for a conclusive statement on either the dipole cross section parametrization or the heavy quarkonium LFWF. For instance, using the boosted Gaussian parametrization given in Ref. [14], the J/Ψ cross section at $Q^2 = 0$ could differ by as much as 30% using dipole cross section parametrizations in Table 1.

On the other hand, one might expect that the quark-antiquark pair originated from quantum fluctuation of the virtual photon scatter universally on the nuclear target for the production of different states of the same quarkonium system, for example, J/Ψ and $\Psi(2s)$ states of charmonium. Under such an assumption, the cross-section ratio of higher excited states over the ground state should exhibit weaker dependence on dipole model than the cross section itself. Our calculations suggest this is indeed the case. In left panel of Fig. 4, we calculate the ratio of the $\Psi(2s)$ cross section to the J/Ψ cross section as a function of Q^2 predicted by the BLFQ LFWF and various dipole cross section parametrizations in Table 1 and 2 for electron-proton collisions. The kinetic variables are chosen to be the mean values of experimental measurements [43]. We observe that the cross-section ratio exhibits weak dependence on dipole models, especially in the large Q^2 regime, where the pQED photon wavefunction in the dipole models we adopted are well motivated by k_t factorization.

In Fig. 4, we also present the BLFQ LFWF predictions for the cross-section ratio $\sigma_{\Psi(2s)}/\sigma_{J/\Psi}$ in electron-gold collisions (middle) and electron-lead collisions (right), with $\Psi(2s)$ and J/Ψ being produced coherently. We use the mean value of W at the HERA experiment of ep collisions after integrating over t. The cross-section ratio for electron-gold collisions to electron-lead collisions also shows weak dependence on the dipole model.

Future electron-ion collision experiments with high luminosity are expected to deliver data on production of higher excited states of heavy quarkonium over a wide kinematic range [11]. The uncertainties

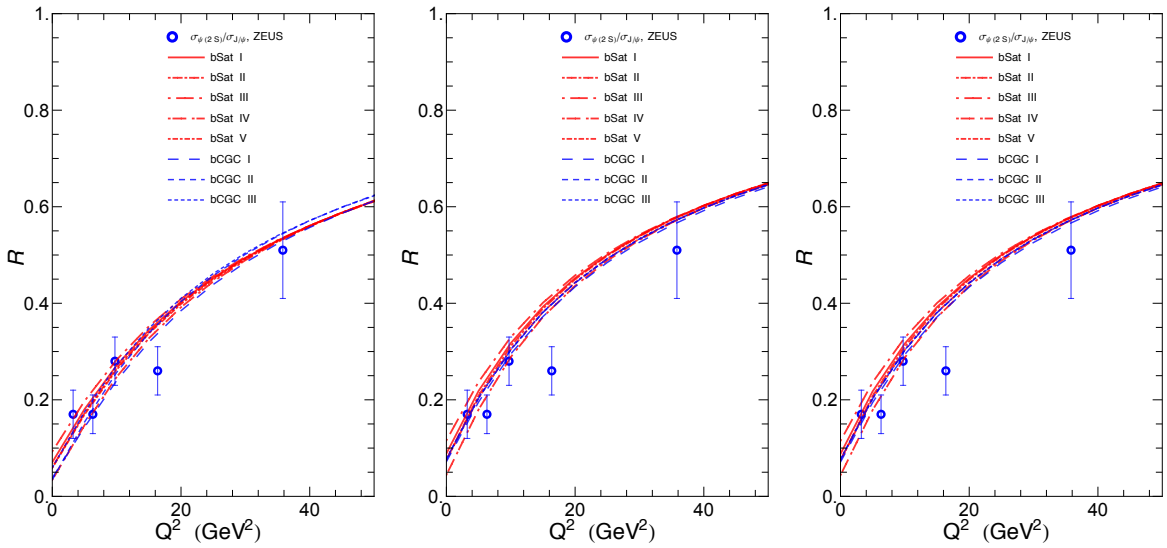

Figure 4: (Colors online) The cross-section ratio $\sigma_{\Psi(2s)}/\sigma_{J/\Psi}$ as a function of Q^2 predicted by BLFQ LFWF and various dipole cross section parametrizations in Table 1 and 2 for electron-proton collision (*Left*), coherent charmonium production in electron-gold collision (*Middle*) and coherent charmonium production in electron-lead collision (*Right*). The cross-section ratio exhibits weak dependence on dipole models. The experimental data points are measurements by ZEUS collaboration [43] in electron-proton scattering at HERA.

associated with heavy quarkonium LFWFs could be reduced through measurements of cross-section ratios of higher excited state to the ground state, owing to its insensitivity to the dipole model. With well-constrained heavy quarkonium LFWFs, the gluon density distribution in the small-x regime could be abstracted efficiently through the diffractive heavy quarkonium production process.

6. Summary and Outlook

Using the dipole models, we study diffractive charmonium production with a theoretical light-front wavefunction obtained from the basis light-front quantization approach. One-gluon exchange dynamics from QCD Lagrangian and effective confining potential inspired by soft-wall light-front holographic QCD are implemented in the effective Hamiltonian. Two parameters in the effective Hamiltonian are fixed by the the mass spectrum of charmonium. The resulting charmonium LFWF gives reasonably good descriptions of currently available experimental data at HERA, RHIC and LHC within the dipole model. We observe that the cross-section ratio of $\sigma_{\Psi(2s)}/\sigma_{J/\Psi}$ as a function of Q^2 has a weak dependence on the dipole model but is rather sensitive to the charmonium wavefunction. We suggest that future electron-ion collision experiments could reduce theoretical uncertainties associated with the structure of heavy quarkonium by measuring the cross-section ratios of the higher excited states to the ground state, owing to their weak dependence on the dipole cross section. Accurate meson wavefunctions will eventually lead to a more precise description of the gluon distribution in the saturation regime [11].

Charmonium production in UPC at LHC has been recorded through proton-proton, proton-lead and lead-lead collisions at various energy scales. We will report theoretical results to compare with these experiments in a separate publication. Upsilon production in UPC at LHC is also under investigation.

The effective Hamiltonian, whose wavefunctions we employ, has been fitted only to the mass spectra of heavy quarkonia. The resulting LFWFs have now been found to provide reasonable descriptions of heavy quarkonia decay constants, form factors and diffractive meson production. Therefore, the BLFQ formalism provides a platform for a unified description of the physical observables mentioned above. Our future goals include improving the effective Hamiltonian of heavy quarkonium using additional experimental measurements as constraints. Using the BLFQ LFWFs to predict diffractive heavy quarkonium production in future electron-ion collision experiments is an important future goal since a large amount

of experimental data, especially data on the production of higher excited heavy quarkonium states, are anticipated.

Acknowledgments

We wish to thank X. Zhao, P. Wiecki and Y. Xie for valuable discussions. We thank N. Kovalchuk for providing us the experimental data for $\Psi(2s)$ measurement. This work was supported in part by the Department of Energy under Grant Nos. DE-FG02-87ER40371 and DESC0008485 (SciDAC-3/NUCLEI). We acknowledge computational resources provided by the National Energy Research Scientific Computing Center (NERSC), which is supported by the Office of Science of the U.S. Department of Energy under Contract No. DE-AC02-05CH11231.

References

[1] L. V. Gribov, E. M. Levin and M. G. Ryskin, Phys. Rept. **100**, 1 (1983).
[2] J. Jalilian-Marian, A. Kovner, L. D. McLerran and H. Weigert, Phys. Rev. D **55**, 5414 (1997).
[3] F. Gelis, E. Iancu, J. Jalilian-Marian and R. Venugopalan, Ann. Rev. Nucl. Part. Sci. **60**, 463 (2010).
[4] K. Golec-Biernat and M. Wüsthoff, Phys. Rev. D **59**, 014017 (1999); K. Golec-Biernat and M. Wüsthoff, Phys. Rev. D **60**, 114023 (1999).
[5] E. Levin and K. Tuchin, Nucl. Phys. A **691**, 779 (2001); E. Levin and K. Tuchin, Nucl. Phys. A **693**, 787 (2001).
[6] E. Gotsman, E. Levin, U. Maor and E. Naftali, Phys. Lett. B **532**, 37 (2002).
[7] H. Kowalski and D. Teaney, Phys. Rev. D **68**, 114005 (2003).
[8] E. Gotsman, E. Levin, M. Lublinsky, U. Maor and E. Naftali, hep-ph/0302010.
[9] E. Iancu, K. Itakura and S. Munier, Phys. Lett. B **590**, 199 (2004).
[10] J. L. Abelleira Fernandez *et al.* [LHeC Study Group Collaboration], J. Phys. G **39**, 075001 (2012).
[11] A. Accardi *et al.*, Eur. Phys. J. A **52**, 268 (2016).
[12] A. H. Mueller, Nucl. Phys. B **335**, 115 (1990).
[13] N. N. Nikolaev and B. G. Zakharov, Z. Phys. C **49**, 607 (1991).
[14] H. Kowalski, L. Motyka and G. Watt, Phys. Rev. D **74**, 074016 (2006).
[15] C. Marquet, Phys. Rev. D **76**, 094017 (2007).
[16] J. P. Vary, H. Honkanen, J. Li, P. Maris, S. J. Brodsky, A. Harindranath, G. F. de Teramond, P. Sternberg, E. G. Ng and C. Yang, Phys. Rev. C **81**, 035205 (2010).
[17] H. Honkanen, P. Maris, J. P. Vary and S. J. Brodsky, Phys. Rev. Lett. **106**, 061603 (2011).
[18] J. P. Vary, L. Adhikari, G. Chen, Y. Li, P. Maris and X. Zhao, Few Body Syst. **57**, 695 (2016).
[19] X. Zhao, H. Honkanen, P. Maris, J. P. Vary and S. J. Brodsky, Phys. Lett. B **737**, 65 (2014).
[20] P. Wiecki, Y. Li, X. Zhao, P. Maris and J. P. Vary, Phys. Rev. D **91**, 105009 (2015) .
[21] L. Adhikari, Y. Li, X. Zhao, P. Maris, J. P. Vary and A. A. El-Hady, Phys. Rev. C **93**, 055202 (2016).
[22] Y. Li, P. Maris, X. Zhao and J. P. Vary, Phys. Lett. B **758**, 118 (2016).
[23] M. G. Ryskin, R. G. Roberts, A. D. Martin and E. M. Levin, Z. Phys. C **76**, 231 (1997).
[24] J. Bartels, K. J. Golec-Biernat and H. Kowalski, Phys. Rev. D **66**, 014001 (2002).
[25] A. H. Rezaeian, M. Siddikov, M. Van de Klundert and R. Venugopalan, Phys. Rev. D **87**, 034002 (2013).
[26] T. Lappi and H. Mantysaari, Phys. Rev. C **83**, 065202 (2011).
[27] T. Toll and T. Ullrich, Phys. Rev. C **87**, 024913 (2013).
[28] T. Lappi and H. Mantysaari, Phys. Rev. C **87**, 032201 (2013).
[29] L.N. Lipatov, Sov. J. Nucl. Phys. **23**, 338 (1976); E.A. Kuraev, L.N. Lipatov and V.S. Fadin, Sov. Phys. JETP **44**, 443 (1976); E.A. Kuraev, L.N. Lipatov and V.S. Fadin,Sov. Phys. JETP **28**, 822 (1978).
[30] E. Levin and K. Tuchin, Nucl. Phys. B **573**, 833 (2000).
[31] I. Balitsky, Nucl. Phys. B **463**, 99 (1996); Y. V. Kovchegov, Phys. Rev. D **60**, 034008 (1999).
[32] G. Soyez, Phys. Lett. B **655**, 32 (2007).
[33] A. H. Rezaeian and I. Schmidt, Phys. Rev. D **88**, 074016 (2013).
[34] G. Watt and H. Kowalski, Phys. Rev. D **78**, 014016 (2008).
[35] G. P. Lepage and S. J. Brodsky, Phys. Rev. D **22**, 2157 (1980).
[36] J. R. Forshaw, R. Sandapen and G. Shaw, Phys. Rev. D **69**, 094013 (2004).
[37] S. J. Brodsky, T. Huang and G. P. Lepage, SLAC-PUB-2540.
[38] J. Nemchik, N. N. Nikolaev, E. Predazzi and B. G. Zakharov, Z. Phys. C **75**, 71 (1997).
[39] S. J. Brodsky, G. F. de Teramond, H. G. Dosch and J. Erlich, Phys. Rept. **584**, 1 (2015).
[40] T. Lappi and H. Mntysaari, PoS DIS **2014**, 069 (2014).
[41] S. Chekanov *et al.* [ZEUS Collaboration], Nucl. Phys. B **695**, 3 (2004).
[42] A. Aktas *et al.* [H1 Collaboration], Eur. Phys. J. C **46**, 585 (2006).
[43] H. Abramowicz *et al.* [ZEUS Collaboration], PoS DIS **2015**, 078 (2015).
[44] C. A. Bertulani, S. R. Klein and J. Nystrand, Ann. Rev. Nucl. Part. Sci. **55**, 271 (2005).
[45] B. Kopeliovich, A. Tarasov and J. Hufner, Nucl. Phys. A **696**, 669 (2001).
[46] V. P. Goncalves, B. D. Moreira and F. S. Navarra, Phys. Rev. C **90**, 015203 (2014).
[47] M. B. G. Ducati, M. T. Griep and M. V. T. Machado, Phys. Rev. C **88**, 014910 (2013).
[48] S. Afanasiev *et al.* [PHENIX Collaboration], Phys. Lett. B **679**, 321 (2009).
[49] A. Takahara, Dissertation, 2013.

[50] E. Abbas *et al.* [ALICE Collaboration], Eur. Phys. J. C **73**, 2617 (2013).
[51] V. Khachatryan *et al.* [CMS Collaboration], [arXiv:1605.06966 [nucl-ex]].
[52] J. Adam *et al.* [ALICE Collaboration], Phys. Lett. B **751**, 358 (2015).